ADSORPTION BEHAVIOR OF CHITOSAN-MWCNTs NANOCOMPOSITE FOR THE ELIMINATION OF OFLOXACIN MEDICATION

Zainab Jasim Khudair [ID][a] and Zeina Mohammad Kadam [b*]

[a] *Department of Science, College of Basic Education, Al-Muthanna University, Al-Qishla str., Samawah, 66001, Iraq*
[b] *Department of Chemistry, College of Science, Al-Qadisiyah University, Um-Alkhail str., Diwaniyah, 58001, Iraq*
[*]e-mail: zeina.m.kadam@qu.edu.iq

Abstract. A nanocomposite of chitosan and poly acrylic acid grafting multi-walled carbon nanotubes p(CS-co-AA)/MWCNTs was produced using free radical polymerization to study its efficiency in eliminating the antibiotic ofloxacin (OFL) from aqueous solutions. The synthesized nanocomposite material has undergone characterization using FTIR, XRD, FESEM, TEM, EDX, and Zeta potential techniques. The adsorption of OFL on the p(CS-co-AA)/MWCNTs has been evaluated using three established Langmuir, Freundlich, and Temkin isotherm models. The isotherm constant (KF) of 0.218 and the separation factor (R^2) of 0.956 indicate strong and desirable adsorption of OFL on p(CS-co-AA)/MWCNTs with a concentration of 100 mg/L at a temperature of 293K and an acidic medium with a pH of 7.0. The primary cause of the reduction in OFL adsorption and dehydrogenation is the increase in pH level. The Van't Hoff equation indicates that the OFL adsorption process exhibits fast kinetics, as seen by a negative thermodynamic parameter ΔH of -0.012 kJ/mol. The pseudo-second-order kinetic model ($R^2 = 1.00$) confirms this observation. The results indicate that the synthesized nanocomposite can effectively remove OFL from polluted aqueous solutions.

Keywords: multi-walled carbon nanotubes, chitosan nanocomposite, ofloxacin drug, adsorption, thermodynamic.

Introduction

Fluoroquinolone antibiotics (FQs) are prevalent antibiotics globally and are extensively employed for treating various microbial illnesses in humans and other species [1]. Nevertheless, individuals only absorb a portion of the antibiotic, with 25-75% of it being expelled into the environment through urine and feces [2]; this leads to the buildup of FQs in the aquatic environment. Ofloxacin (OFL) is a quinolone antibiotic with a wide range of activity inhibiting bacteria's DNA gyrase. It can be administered in several dosage forms [3]. Currently, the techniques used to eliminate FQs from water include adsorption, oxidation, photocatalysis, and biodegradation [4]. Adsorption has become a prominent focus of studies because of its simplicity, cost-effectiveness, and lack of harmful by-products that might lead to more pollution. Consequently, it has emerged as the predominant technique for eliminating antibiotics from water [5,6].

The adsorption method can effectively treat a diverse array of pollutants. This method is considered the most economical, effective, practical, and environmentally benign of the currently employed wastewater treatment technologies [7-9]. Adsorption is a widely recognized surface phenomenon that can effectively eliminate organic and inorganic micropollutants. It removes impurities from water after chemical or biological treatment. Adsorption is increasingly employed to remove dissolved contaminants that have resisted chemical oxidation or biological treatment [10-12].

A variety of adsorbents have been employed for the purpose of antibiotic adsorption from its aqueous environment, including carbon nanotubes, activated carbon, ion exchange resins, clay minerals, and biochar, which has recently garnered considerable interest owing to its abundant supply and reasonable price [13]. Carbon nanotubes (CNTs) possess a great capacity to adsorb heavy metals and persistent organic pollutants because of their strong hydrophobic nature and extensive surface area (SA). As a result, CNTs are being progressively employed as adsorbents in the process of removing pollutants [14-16]. Multi-walled carbon nanotubes (MWCNTs) are a form of carbon nanotubes that consist of two or more carbon sheets and have a diameter ranging

from 1 to 20 nm [17]. They are commonly used to adsorb medicines [18], organic compounds [19] and surfactants [20] from aqueous solutions. CNTs are a highly promising type of adsorbent for the purification of water. Nevertheless, the effectiveness of their application is constrained by the propensity for aggregating up and the inability to recover from such conditions [21]. Surface functionalization and/or integration with other materials are considered effective strategies to address these restrictions [22]. Chitosan (CS) is a biopolymer derived from chitin, with abundant amine and hydroxyl functional groups. It has gained significant interest due to its strong binding ability, wide availability, and remarkable film-forming properties [23].

The present research aims to assess the feasibility of utilizing MWCNTs combined with poly chitosan and acrylic acid nanocomposites as an adsorbent for OFL adsorption, evaluate the suitability of different isotherm models (such as Langmuir and Freundlich) to identify the best-suited isotherm equation and determine kinetic parameters and the adsorption mechanism. The impact of many factors, such as adsorbent amount, contact duration, pH, and temperature, on the adsorption process has been investigated.

Experimental
Materials

The MWCNTs powder (OD= 40–60 nm, length= 5–10 um, purity 99%, surface area> 200m^2/g, layers number= 7, density 2.1 g/cm^3), was obtained from VCN Materials, Co., Ltd, Iran. Chitosan (CS) with a median molecular weight of 96% acquired from HIMEDIA, India. The OFL medication was provided by MACLIN, China. Acrylic acid (AA) was acquired from Merck, Germany. Acetic acid with a purity of 99.5% and *N,N'*-methylenebisacrylamide (MBA) with a purity of 99% were obtained from CDH, India. The initiator, potassium persulfate (KPS) with a purity of 99%, has been obtained from THOMAS BAKER, India. The chemicals: NaCl, CaCl$_2$, KCl, NaOH, HCl, and N$_2$ gas have been supplied from Fluka, Germany. All the solutions were diluted using de-ionized water.

Preparation of poly (CS-co-AA)/MWCNTs nanocomposites

To make a 2.5 wt% CS solution, 0.5 g of CS was mixed with 20 mL of 1% acetic acid. The dispersal of CS polymer was finished by stirring the resulting solution for 15 minutes at 60°C. Before being introduced to the CS solution, a 0.1% MWCNT solution was treated for 10 minutes under an ultrasonic field. Stirring the

CS/MWCNTs mixture at 70°C ensured that the grafting process was finished. As a polymer cationic surfactant, CS macromolecules were adsorbed onto the MWCNTs' surface during this stage, stabilizing the MWCNTs [24].

The preceding solution was supplemented with 15 mL of acrylic acid (AA) as a monomer. After adding the initiator KSP (0.02 g in 2 mL DI.W.) and the cross-linker MBA (0.02 g in 2 mL DI.W.), stirring continuously, the solution was bubbled with nitrogen gas for 15 minutes to remove any oxygen and then placed in a water bath at 65°C for two hours to finish the polymerization process. The final nanocomposite material was cut into five mm-sized pieces and continuously rinsed with deionized water, then refilled with fresh deionized water for 24 hours to eliminate unreacted monomers. The nanocomposite material was rinsed and then dried at 50°C to a consistent weight. Ultimately, p(CS-co-AA)/MWCNTs were crushed, sieved, and kept in airtight containers for further use [25].

Instruments

FT-IR spectra for nanocomposites were registered on a Bruker, Germany (model: Equinox 55, Tensor 27), KBr at a range of (400-4000 cm^{-1}). *XRD* collected from a diffractometer of the Philips, USA (model: PW1730). *Microscopic study* of the products was indicated by FESEM with Tescan, Czech Republic (model: Mira3) and TEM *via* Philips, Nederland (model: EM20.8S). Zeta potential was determined using Malvern Instrument Zetasizer Nano-ZS. EDX is the same as FESEM device and only detector changes (SE). *UV-Vis* spectra were conducted on a Shimadzu, Japan ultraviolet-visible spectrophotometer (model: PC 1800)

Adsorption isotherm

Initial data were gathered by batch adsorption experiments, which helped determine the best concentration, equilibrium duration, temperature, ionic strength, and pH for maximal removal effectiveness. All tests were conducted three times each. All tests were conducted three times each, in separate stoppered conical flasks, each set containing 0.05 g of nanocomposites. A quantity of 10 mL of a prepared OFL drug solution at concentration of 100 mg/L was added to each flask. After the samples were shaken at 125 rpm in the shaking incubator until equilibrium was reached, they were centrifuged at 3000 rpm for ten minutes to separate them. The equilibrium concentrations (C$_e$) were determined using the calibration curve. The amount of drug absorbed was determined using Eq.(1) [26].

$$Qe \ or \ \frac{x}{m} = \frac{V(Co-Ce)}{m} \quad (1)$$

The adsorption efficiency (E%) of the drug was calculated according to the Eq.(2) [27,28].

$$E\% = \frac{Co-Ce}{Co} \times 100 \quad (2)$$

where, x is the amount of adsorbed drug;
m (g) is the mass of the adsorbent material;
Q_e (mg/g) is the quantity of drug adsorbed at equilibrium;
C_o (mg/L) and C_e (mg/L) refer to the initial and at equilibrium concentrations of the drug, respectively.

Results and discussion
Characterization of p(CS-co-AA)/MWCNTs nanocomposites

The FTIR spectrum of the p(CS-co-AA)/MWCNTs nanocomposites is shown in Figure S1. The spectrum indicates the presence of a peak in 1147 cm^{-1} of the C-O group tensile vibration in chitosan. Peak appearance at 1706 cm^{-1} illustrates C=O of the acrylic acid, and the adsorption bands at 2931 cm^{-1} illustrate the aliphatic C-H tensile group in acrylic acid. The prominent band observed in the spectrum, spanning from around 2500 to 3500 cm^{-1}, can be attributed to the hydrogen bonding present in the composite.

Figure S2 shows the XRD patterns of p(CS-co-AA)/MWCNTs nanocomposites. The lack of sharp diffraction patterns indicates on the amorphous nature of the sample which only had a broad diffraction band of 20.05 at 2θ angle, characteristic for amorphous chitosan composite. Also, the peak in position 36.1 demonstrates the presence of polyacrylic acid in this nanocomposite material. This is similar to the observation made for amorphous chitosan composite by [29].

Figure 1(*a*) displays the scanning electron microscope (SEM) images of the p(CS-co-AA)/MWCNTs, the composites have a rough non-smooth surface, which increases the specific surface area. This, in turn, improves the efficiency of adsorption. Additionally, the presence of porosity can be observed on the surface of the p(CS-co-AA)/MWCNTs, leading to enhanced adsorbent characteristics. Figure 1(*b*) is a TEM micrographs of p(CS-co-AA)/MWCNTs composite. TEM images of nanocomposites showed no discernible MWCT, indicating a high degree of homogeneity and a significant impact of chitosan on carbon nanotubes. The micrographs showed a porous and hollow structure, the particles are of irregular shapes, lines of aligned pores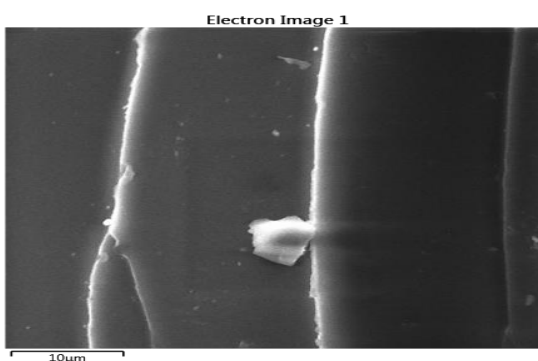 are visible, indicating the existence of a highly porous architecture which had resulted in p(CS-co-AA)/MWCNTs having a high specific surface area.
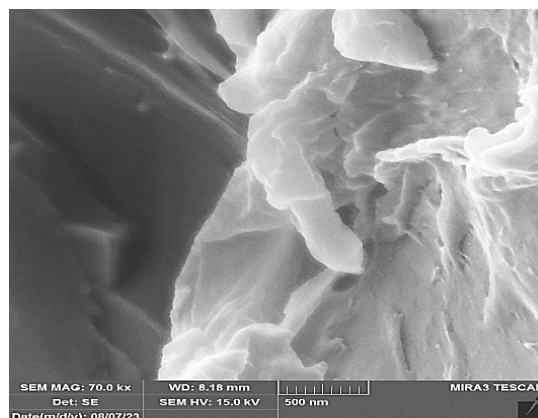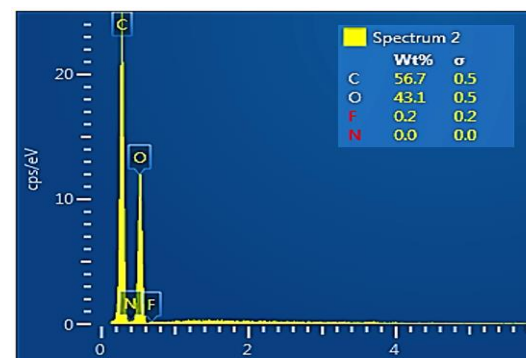

(a)
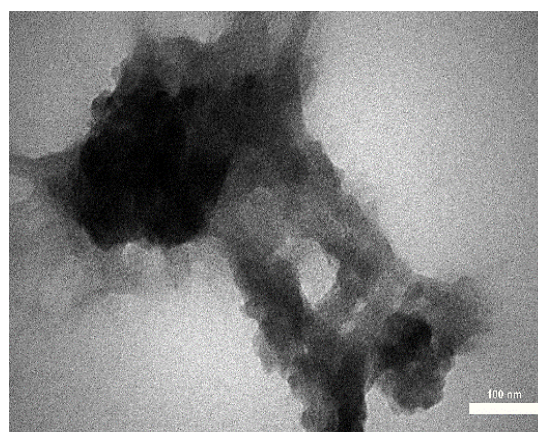
(b)

(c)

(d)

Figure 1. Micrographs of p(CS-co-AA)/MWCNTs FESEM (*a*), TEM (*b*), EDS (*c,d*).

Both SEM and TEM micrographs, in general supported the amorphous nature of the surface. Figure 1(c) displays the EDS (energy dispersive spectrometry) analysis; the percentage values of the elements in the composites are shown Figure 1(d).

The zeta potential of the p(CS-co-AA)/ MWCNTs nanocomposites is determined to be -46.5 mV, indicating a significant anionic charge. This is illustrated in Figure S3. The existence of oxygen-containing groups, such as carboxyl and carbonyl on the surface of untreated powders is responsible for the negative zeta potential values in chitosan and acrylic acid. The negative zeta potential of the nanocomposite surface can be attributed to the dissociation of the carboxyl (COOH) and carbonyl (C=O) groups [30].

Adsorption study

Calibration curve of OFL drug

The OFL drug was serially diluted to create solutions of various concentrations. The absorption values of OFL solutions were measured at the chosen wavelength (λ_{max}= 287 nm). These values were then plotted against the concentration values of OFL, as depicted in Figure S4. The calibration curve was used to determine the OFL's concentration within the range where Beer-Lambert's law is applicable.

Effect of contact time

Figure 2 indicates the effect of contact time on drug adsorption by p(CS-co-AA)/MWCNTs nanocomposites. The amount of drug adsorbed increases rapidly, being noticeable during the first 10 min. The amount of drug adsorbed increases gradually until the contact time is reached, that indicates that all the active groups are saturated with the adsorbent material. At the duration of 90 minutes, a small alteration in the quantity of adsorbed drug was observed. Therefore, this time point was selected as the optimal adsorption time for the drug, utilizing the p(CS-co-AA)/MWCNTs nanocomposites [31].

Effect of temperature

Temperature's impact on the adsorption was studied at 15-30°C, several concentrations of the drug (in the range of 10–200 mg/L) being taken. The contact time was of 90 min. The results shown in Figure 3 demonstrate that the concentration of OFL drug increases once the temperature decreases, which indicates that the adsorption process is exothermic. The greater kinetic energy of the molecules and their reduced propensity to interact with the adsorbent may be associated with the temperature of the adsorption process. At ambient temperatures, the amount of OFL

adsorbed is acceptable compared to data obtained at higher temperatures, and the decrease does not appear to be significant within the range of 15-30°C [32,33].

Effect of pH

The findings on the determination of the efficacy of p(CS-co-AA)/MWCNTs nanocomposites in removing OFL are displayed in Figure 4. Results were obtained by using solutions of HCl (0.1 mol/L) and NaOH (0.1 mol/L) in a pH range of 2-10. Data demonstrated an increase in removal efficiency in the pH range 2–7.
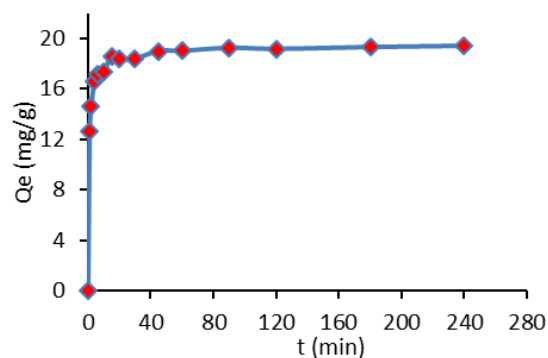

Figure 2. The effect of contact time on OFL adsorption on the p(CS-co-AA)/MWCNTs at 20°C, 90 min, pH= 7.
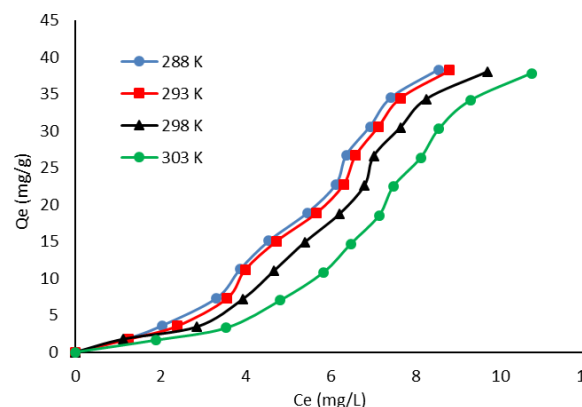

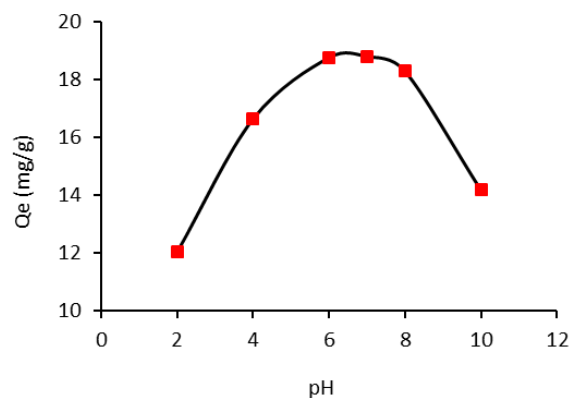**Figure 3. Effect of temperature on the adsorption of OFL on the p(CS-co-AA)/ MWCNTs.**

Figure 4. Effect of pH in the OFL adsorption on the p(CS-co-AA)/ MWCNTs.
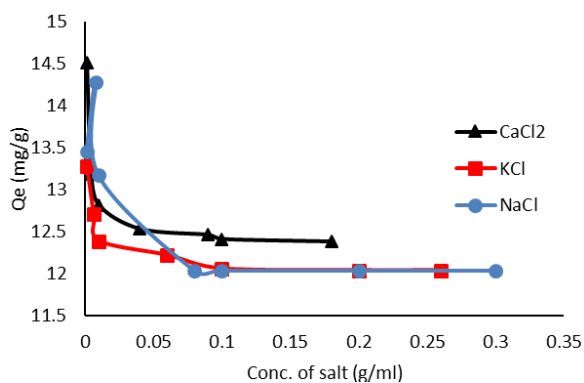
Figure 5. Effect of ionic strength on the OFL adsorption on the p(CS-co-AA)/ MWCNTs.
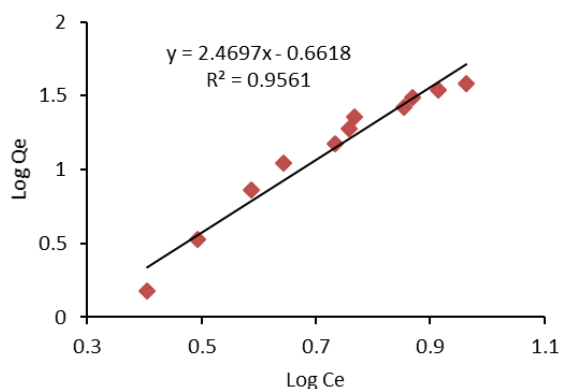

Figure 6. Freundlich isotherm for adsorption of OFL onto p(CS-co-AA)/MWCNTs at 20°C, 90 min, pH= 7.

The most efficient removal of OFL was observed at pH 7, according to the experiments. This is due to the fact that adsorbates become ionized and acquire a negative charge at this pH [33]. The adsorbent forms an electrostatic interaction with drug because of the positive charges of the chitosan and polyacrylic acid. This is because NH_2 group of the chitosan and the COOH group of the polyacrylic acid both become positively charged and release NH_3^+ and $COOH_2^+$, respectively, in the aqueous solution. Additionally, when the pH is greater than the pka values (pka, OFL= 6.08), the drug is protonated, and the adsorbents' positive charges provide a repulsive force, resulting in reduced adsorption at higher pH values [34].

Effect of ionic strength

Figure 5 shows that the amount of adsorbent material decreases with the increase of the salt concentration. To interpret this phenomenon, if the nature of the linkages between the adsorbent and adsorbate is electrostatic attraction, the efficiency of the adsorption process will be reduced, addition occurs competitive between salt ions and cationic drug molecules. The salt also creates double layer, disrupting the drug from its adhesion to the surface [35]. It can also be noticed that the effect of calcium ion is lower than the rest due to the smaller size of the ionic radius. Also, the higher electrostatic attraction of the sodium and potassium ions will increase the shielding effect on the surface of nanocomposites, that leads to reduction of the adsorption process.

Adsorption isotherm models

The relationship between the amount of material adsorbed and the concentration of the adsorbate in the solution, with regards to temperature, is described by the adsorption isotherm. The adsorption equilibrium data were analysed using the Freundlich, Temkin, and Langmuir isotherms. The correlation coefficients are typically used to determine the appropriateness of isotherm equations and establish a linear relationship. The Freundlich isotherm expresses a direct correlation between log C_e and log Qe. The isotherm depicted in Figure 6 (Langmuir and Temkin plots shown in Figure S5 and S6, respectively) and Table 1 demonstrates that OFL drug ions apply to this isotherm depending on the correlation coefficient. This suggests that the surface is heterogeneous and multi-layer with a difference in energy levels between active adsorption sites. The Langmuir adsorption isotherm describes the formation of a monolayer of adsorbate molecules on a surface, with an equal number of adsorption sites [36].

Adsorption thermodynamics

The basic thermodynamic quantities of adsorption of OFL drug on p(CS-co-AA)/MWCNTs nanocomposites were estimated *via* calculating values X_m at several solution temperatures (Figure 7). The free change energy (ΔG), entropy (ΔS) and enthalpy (ΔH) are calculated using Eqs.(3-5).

$$\Delta G = \Delta H - T \times \Delta S \qquad (3)$$

$$\Delta G = -RT \ln Keq \qquad (4)$$

$$\ln Keq = -\frac{\Delta H°}{RT} + \frac{\Delta S°}{R} \qquad (5)$$

Table 1

The coefficients and constants of correlation Langmuir, Friendlies and Temkin isotherms of OFL adsorption on the p(CS-co-AA)/ MWCNTs.

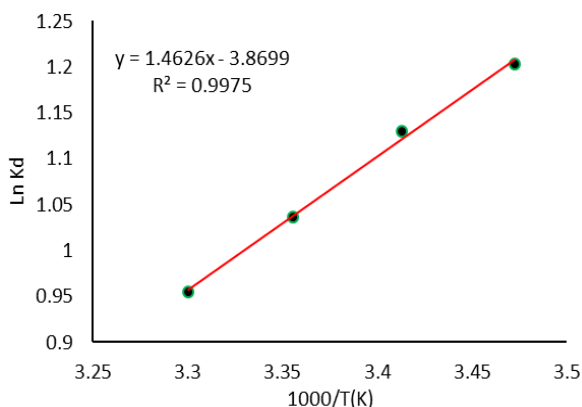| Langmuir equation			Freundlich equation			Temkin equation		
K_L	Q_{max}	R^2	K_F	n	R^2	K_T	B	R^2
-0.077	-20.964	0.7096	0.218	0.405	0.9561	0.3559	29.842	0.9497

Figure 7. Plot of ln Xm against reciprocal absolute temperature for adsorption of OFL drug adsorption on the p(CS-co-AA)/ MWCNTs.

Table 2 shows the thermodynamic parameter of OFL drug adsorption on the surface of p(CS-co-AA)/MWCNTs nanocomposites; Free Gibbs energy (ΔG) has a negative value indicating that the adsorption process is (spontaneous) [37]. While the change in entropy (ΔS), the negative value indicates that the particles adsorbed on the surface of the adsorbent polymer are more regular and that the particles are restricted in movement. As for the change in enthalpy (ΔH), its negative value indicates that the adsorption process is exothermic, and since the enthalpy value is less than 40 KJ/mol, the adsorption process of OFL on the surface of the nanocomposite is of a physical nature.

Adsorption kinetics

Key to the kinetic process is comprehending the dynamic response and investigating adsorption conditions. In order to determine the control phase and adsorption mechanism, experimental data has been analysed using a variety of kinetic models. Various models, such as intraparticle diffusion, pseudo-first-order, and pseudo-second-order kinetic models, were used to determine the adsorption process kinetic equation.

The pseudo-first-order kinetic model is represented in Eq.(6) [38].

$$Ln(qe - qt) = ln(qe) - k_l * t \qquad (6)$$

The linear plot $\ln(q_e - q_t)$ as a function of t is presented. The corresponding data is also recorded in Table 3 and Figure 8*(a)* for the (OFL). According to the pseudo-first-order kinetic model, the number of available vacant spaces has a direct correlation with the rate of filling the adsorbent active sites. Table 3 shows that there is a disagreement between the results and experimental data derived from the pseudo-first order kinetic model and the equilibrium adsorption capacity values (q_e) for OFL. The q_e values from the model do not match the experimental values (q_{exp}).

According to the pseudo-second-order model, the adsorbent and adsorbate share or exchange electrons, which controls the rate of surface adsorption. Eq.(7) represents the form of the pseudo-second-order [39].

$$\frac{1}{q} = \frac{1}{kh.qe2} + \frac{t}{qe} \qquad (7)$$

where, k_h is a pseudo-second-order constant, (g/mg.min).

By plotting the OFL adsorption on the p(CS-co-AA)/MWCNTs nanocomposites and then determining the slope and intercept of the lines at different concentrations, the values of q_e and k_h have been ascertain, as shown in Table 3 and Figure 8*(b)*. The pseudo-second-order equation appears to be an appropriate model for depicting the OFL kinetics process on the p(CS-co-AA)/MWCNTs nanocomposites, as there is minimal discrepancy between the experimental adsorption capacity (q_{exp}) and the value computed using the model (q_{cal}) along with a higher correlation coefficient compared to other kinetic models.

Table 2

Thermodynamic parameters of OFL drug adsorption on the p(CS-co-AA)/ MWCNTs.

parameter	ΔG (kJ/mol)	ΔH (kJ/mol)	ΔS (J/mol.K)	Equilibrium Constant (K)
OFL – [p(CS-co-AA)/ MWCNTs]	-2.7514	-0.0121	-32.174	3.09408

Table 3

The pseudo-first-order and pseudo-second-order kinetic constants and correlation coefficients of OFL drug adsorption on the p(CS-co-AA)/ MWCNTs.

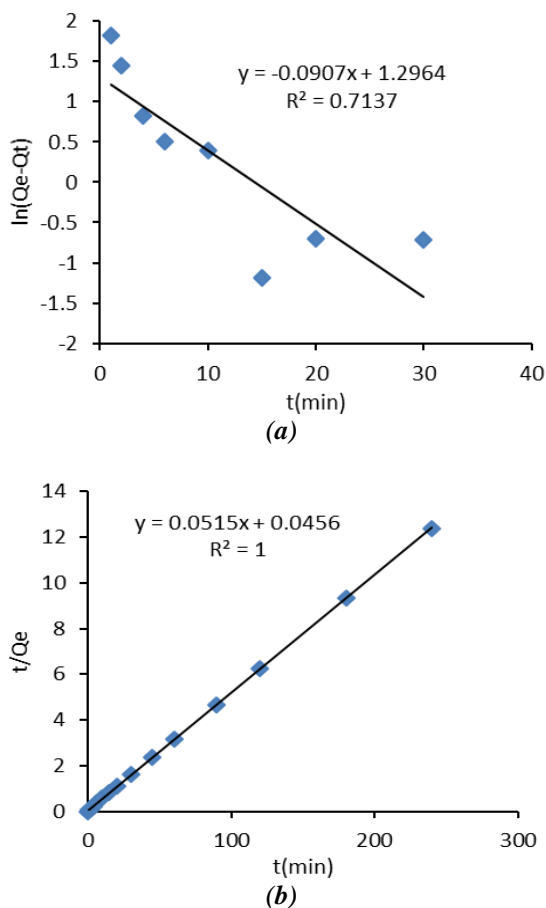| Pseudo-first-order			Pseudo-second-order		
K_1	q_e	R^2	K_2	q_e	R^2
0.091	3.656	0.7137	0.058	19.417	1

Figure 8. Pseudo first order model *(a)*, **Pseudo second order model** *(b)* **of OFL drug adsorption on the p(CS-co-AA)/ MWCNTs.**

Conclusions

MWCNTs combined with poly chitosan and acrylic acid nanocomposites were successfully synthesized and efficiently used for the adsorption of OFL from aqueous solutions. The calculated adsorption parameters and the equilibrium data were best fitted by the Freundlich model, giving a maximum adsorption capacity of 38.8 mg/g in contact time= 120 min, an initial adsorbate concentration= 100 mg/L, and a pH= 7 at 293K (the adsorption capacity decreases as the temperature increases). The authors studied the adsorption process kinetically and analysed the results using pseudo-first-order and pseudo-second-order models. Pseudo-second-order was found to be the best correlation model based on the values of the correlation coefficient (R^2). Negative values of thermodynamic parameters (ΔG= −2.751 and ΔH= −0.012 kJ.mol^{-1}) suggest that this adsorption is exothermic. This result suggests that the p(CS-co-AA)/ MWCNTs nanocomposites prepared in this study could be a promising adsorbent for OFL medication removal in aqueous environments in terms of high efficiency and feasibility.

Supplementary information

Supplementary data are available free of charge at http://cjm.ichem.md as PDF file.

References
1. Izadi, P.; Izadi, P.; Salem, R.; Papry, S.A.; Magdouli, S.; Pulicharla, R.; Brar, S.K. Non-steroidal anti-inflammatory drugs in the environment: Where were we and how far we have come? Environmental Pollution, 2020, 267, 115370, pp. 1–19.
DOI: https://doi.org/10.1016/j.envpol.2020.115370
2. Sciscenko, I.; Thị Mỹ Hằng, H.; Escudero-Oñate, C.; Oller, I;. Arques, A. Fluorescence spectroscopy and chemometrics: a simple and easy way for the monitoring of fluoroquinolone mixture degradation. ACS omega, 2021, 6(7), pp. 4663–4671.
DOI: https://doi.org/10.1021/acsomega.0c05370
3. Rusu, A.; Munteanu, A.C.; Arbănași, E.M.; Uivarosi, V. Overview of side-effects of antibacterial fluoroquinolones: new drugs versus old drugs, a step forward in the safety profile? Pharmaceutics, 2023, 15(3), pp.804–866. DOI: https://doi.org/10.3390/pharmaceutics15030804
4. Pretali, L.; Fasani, E.; Sturini, M. Current advances on the photocatalytic degradation of fluoroquinolones: photoreaction mechanism and environmental application. Photochemical & Photobiological Sciences, 2022, 21(5), pp. 899–912. DOI: https://doi.org/10.1007/s43630-022-00217-z
5. Ma, Y.; Lu, T.; Yang, L.; Wu, L.; Li, P.; Tang, J.; Chen, Y.; Gao, F.; Cui, S.; Qi, X.; Zhang, Z. Efficient adsorptive removal of fluoroquinolone antibiotics from water by alkali and bimetallic salts co-hydrothermally modified sludge biochar. Environmental Pollution, 2022, 298, 118833. DOI: https://doi.org/10.1016/j.envpol.2022.118833
6. Barquilha, C.E.R.; Braga, M.C.B. Adsorption of organic and inorganic pollutants onto biochars: Challenges, operating conditions, and mechanisms. Bioresource Technology Reports, 2021, 15, 100728, pp. 1–15.
DOI: https://doi.org/10.1016/j.biteb.2021.100728
7. Akhtar, L.; Ahmad, M.; Iqbal, S.; Abdelhafez, A.A.; Mehran, M.T. Biochars' adsorption performance towards moxifloxacin and ofloxacin in aqueous solution: Role of pyrolysis temperature and biomass type. Environmental Technology & Innovation, 2021, 24, 101912, pp. 1–15.
DOI: https://doi.org/10.1016/j.eti.2021.101912
8. Saravanakumar, K.; Naveen Prasad, B.S.; Senthilkumar, R.; Reddy Prasad, D.M.; Venkatesan, D. Single and competitive sorption potential of date seed-derived biochar during removal of lead (II) and cadmium (II) ions. Environmental Progress & Sustainable Energy, 2021, 40(6), e13690, pp. 1–10. DOI: https://doi.org/10.1002/ep.13690

9. Rashid, R.; Shafiq, I.; Akhter, P.; Iqbal, M.J.; Hussain, M. A state-of-the-art review on wastewater treatment techniques: the effectiveness of adsorption method. Environmental Science and Pollution Research, 2021, 28, pp. 9050–9066. DOI: https://doi.org/10.1007/s11356-021-12395-x

10. Bartolomeu, M.; Neves, M.G.P.M.S.; Faustino, M.A.F.; Almeida, A. Wastewater chemical contaminants: Remediation by advanced oxidation processes. Photochemical & Photobiological Sciences, 2018, 17(11), pp. 1573–1598. DOI: https://doi.org/10.1039/C8PP00249E

11. Ratnam, M.V.; Akilamudhan, P.; Kumar, K.S.; Reddy, S.N.; Rao, K.N.; Shaik, F.; Prasad, D.M.R. Carbon-based nanoadsorbents for the removal of emerging pollutants. Adsorption Science & Technology, 2023, pp. 1–12. DOI: https://doi.org/10.1155/2023/3579165

12. Ahmed, M.B.; Zhou, J.L.; Ngo, H.H.; Guo, W.; Thomaidis, N.S.; Xu, J. Progress in the biological and chemical treatment technologies for emerging contaminant removal from wastewater: A critical review. Journal of Hazardous Materials, 2017, 323A, pp. 274–298. DOI: https://doi.org/10.1016/j.jhazmat.2016.04.045

13. Mangla, D.; Annu; Sharma, A.; Ikram, S. Critical review on adsorptive removal of antibiotics: Present situation, challenges and future perspective. Journal of Hazardous Materials, 2022, 425, 127946. DOI: https://doi.org/10.1016/j.jhazmat.2021.127946

14. Ashiq, A.; Vithanage, M.; Sarkar, B.; Kumar, M.; Bhatnagar, A.; Khan, E.; Xi, Y.; Ok, Y.S. Carbon-based adsorbents for fluoroquinolone removal from water and wastewater: A critical review. Environmental Research, 2021, 197, 111091, pp. 1–20. DOI: https://doi.org/10.1016/j.envres.2021.111091

15. Zhang, W.; Qiu, X.; Wang, C.; Zhong, L.; Fu, F.; Zhu, J.; Zhang, Z.; Qin, Y.; Yang, D.; Xu, C.C. Lignin derived carbon materials: current status and future trends. Carbon Research, 2022, 1(1), 14. DOI: https://doi.org/10.1007/s44246-022-00009-1

16. Duarte, E.D.V.; Oliveira, M.G.; Spaolonzi, M.P.; Costa, H.P.S.; da Silva, T.L.; da Silva, M.G.C.; Vieira, M.G.A. Adsorption of pharmaceutical products from aqueous solutions on functionalized carbon nanotubes by conventional and green methods: A critical review. Journal of Cleaner Production, 2022, 372, 133743. DOI: https://doi.org/10.1016/j.jclepro.2022.133743

17. Bhuyan, A.; Ahmaruzzaman, M. Recent advances in new generation nanocomposite materials for adsorption of pharmaceuticals from aqueous environment. Environmental Science and Pollution Research, 2023, 30, pp. 39377–39417. DOI: https://doi.org/10.1007/s11356-023-25707-0

18. Ramachandran, K.; Boopalan, V.; Bear, J.C.; Subramani, R. Multi-walled carbon nanotubes (MWCNTs)-reinforced ceramic nanocomposites for aerospace applications: a review. Journal of Materials Science, 2022, 57(6), pp. 3923–3953. DOI: https://doi.org/10.1007/s10853-021-06760-x

19. Hsu, C.Y.; Rheima, A.M.; Mohammed, M.S.; Kadhim, M.M.; Mohammed, S.H.; Abbas, F.H.; Abed, Z.T.; Mahdi, Z.M.; Abbas, Z.S.; Hachim, S.K.; Ali, F.K.; Mahmoud, Z.H.; Kianfar, E. Application of carbon nanotubes and graphene-based nanoadsorbents in water treatment. BioNanoScience, 2023, 13(4), pp. 1418–1436. DOI: https://doi.org/10.1007/s12668-023-01175-1

20. Gan, G.; Fan, S.; Li, X.; Zhang, Z.; Hao, Z. Adsorption and membrane separation for removal and recovery of volatile organic compounds. Journal of Environmental Sciences, 2023, 123, pp. 96–115. DOI: https://doi.org/10.1016/j.jes.2022.02.006

21. Cao, H.; Zhou, Z.; Wang, C.; Sun, H. Adsorption of phenanthrene on multi-walled carbon nanotubes in the presence of nonionic surfactants. International Journal of Environmental Research and Public Health, 2023, 20(4), p.3648. DOI: https://doi.org/10.3390/ijerph20043648

22. Vandenabeele, C.R.; Lucas, S. Technological challenges and progress in nanomaterials plasma surface modification– A review. Materials Science and Engineering: R: Reports, 2020, 139, 100521, pp. 1–40. DOI: https://doi.org/10.1016/j.mser.2019.100521

23. Bazrafshan, E.; Azqhandi, M.H.A.; Foroughi, M.; Gholami, Z. β-cyclodextrin grafted multi-walled carbon nanotubes/chitosan (MWCNT/Cs/CD) nanocomposite for treatment of methylene blue-containing aqueous solutions. Environmental Research, 2023, 231(3), 116208. DOI: https://doi.org/10.1016/j.envres.2023.116208

24. Joseph, S.M.; Krishnamoorthy, S.; Paranthaman, R.; Moses, J.A.; Anandharamakrishnan, C. A review on source-specific chemistry, functionality, and applications of chitin and chitosan. Carbohydrate Polymer Technologies and Applications, 2021, 2, 100036, pp. 1–14. DOI: https://doi.org/10.1016/j.carpta.2021.100036

25. Liu, Y.; Tang, J.; Chen, X.; Xin, J.H. Decoration of carbon nanotubes with chitosan. Carbon, 2005, 43(15), pp. 3178–3180. DOI: https://doi.org/10.1016/j.carbon.2005.06.020

26. Wang, Z.; Ning, A.; Xie, P.; Gao, G.; Xie, L.; Li, X.; Song, A. Synthesis and swelling behaviors of carboxymethyl cellulose-based superabsorbent resin hybridized with graphene oxide. Carbohydrate polymers, 2017, 157, pp. 48–56. DOI: https://doi.org/10.1016/j.carbpol.2016.09.070

27. Hadi, A.A.; Ali, A.A.; Khathi, M.T. Desulfurization of crude oil by laboratory developed multipumping flow injection analysis system with optimization by response surface methodology. Journal of Ecological Engineering, 2023, 24(2), pp. 328–339. DOI: https://doi.org/10.12911/22998993/156662

28. Enayatpour, B.; Rajabi, M.; Yari, M.; Mirkhan, S.M.R.; Najafi, F.; Moradi, O.; Bharti, A.K.; Agarwal, S.; Gupta, V.K. Adsorption/desorption study of proteins onto multi-walled carbon nanotubes and amino multi-walled carbon nanotubes

surfaces as adsorbents. Journal of Molecular Liquids, 2017, 231, pp. 566–571.
DOI: https://doi.org/10.1016/j.molliq.2017.02.013

29. Xu, Y.; Lin, W.; Wang, H.; Guo, J.; Yuan, D.; Bao, J.; Sun, S.; Zhao, W.; Zhao, C. Dual-functional polyethersulfone composite nanofibrous membranes with synergistic adsorption and photocatalytic degradation for organic dyes. Composites Science and Technology, 2020, 199, 108353, pp. 1–10. DOI: https://doi.org/10.1016/j.compscitech.2020.108353

30. Liu, Q.; Xu, K.; Hu, G.; Zeng, F.; Li, X.; Li, C.; Zhang, Y. Underwater superelastic MOF/polyacrylamide/chitosan composite aerogel for efficient 2,4-dichlorophenoxyacetic acid adsorption. Colloids and Surfaces A: Physicochemical and Engineering Aspects, 2022, 635, 127970. DOI: https://doi.org/10.1016/j.colsurfa.2021.127970

31. Gines, L.; Mandal, S.; Ahmed, A.I.; Cheng, C.L.; Sow, M.; Williams, O.A. Positive zeta potential of nanodiamonds. Nanoscale, 2017, 9(34), pp. 12549–12555.
DOI: https://doi.org/10.1039/C7NR03200E

32. Oliveira, M.G.; Spaolonzi, M.P.; Duarte, E.D.V.; Costa, H.P.S.; da Silva, M.G.C.; Vieira, M.G.A. Adsorption kinetics of ciprofloxacin and ofloxacin by green-modified carbon nanotubes. Environmental Research, 2023, 233, 116503.
DOI: https://doi.org/10.1016/j.envres.2023.116503

33. Rowley-Neale, S.J.; Randviir, E.P.; Dena, A.S.A.; Banks, C.E. An overview of recent applications of reduced graphene oxide as a basis of electroanalytical sensing platforms. Applied Materials Today, 2018, 10, pp. 218–226.

34. Karimi, S.; Namazi, H. Magnetic alginate/glycodendrimer beads for efficient removal of tetracycline and amoxicillin from aqueous solutions. International Journal of Biological Macromolecules, 2022, 205, pp. 128–140. DOI: https://doi.org/10.1016/j.ijbiomac.2022.02.066

35. Hasanzadeh, V.; Rahmanian, O.; Heidari, M. Cefixime adsorption onto activated carbon prepared by dry thermochemical activation of date fruit residues. Microchemical journal, 2020, 152, 104261.
DOI: https://doi.org/10.1016/j.microc.2019.104261

36. Hu, Z.; Chen, H.; Ji, F.; Yuan, S. Removal of Congo Red from aqueous solution by cattail root. Journal of Hazardous materials, 2010, 173(1-3), pp. 292–297. DOI: https://doi.org/10.1016/j.jhazmat.2009.08.082

37. Tian, W.; Deng, Z.; Wang, H.; Liu, H.; Li, G.; Liu, X.; Chen, Z.; Chen, H.; Li, Y. Negative adsorption in the isotherm adsorption experiments of low-adsorption coal and shale. Natural Gas Industry B, 2019, 6(1), pp. 44–50.
DOI: https://doi.org/10.1016/j.ngib.2019.01.006

38. Rassaei, F. Kinetics, isotherms, thermodynamic adsorption, and desorption studies of chromium in two types of calcareous soils. Arabian Journal of Geosciences, 2023, 16(3), 214.
DOI: https://doi.org/10.1007/s12517-023-11291-7

39. Revellame, E.D.; Fortela, D.L.; Sharp, W.; Hernandez, R.; Zappi, M.E. Adsorption kinetic modeling using pseudo-first order and pseudo-second order rate laws: A review. Cleaner Engineering and Technology, 2020, 1, 100032, pp. 1–13.
DOI: https://doi.org/10.1016/j.clet.2020.100032